JOINT EUROPEAN TORUS JET

JET–P(91)60

A. Loarte, P.J. Harbour
and JET Team

The Effect of the Magnetic Flux Geometry of a Poloidal Divertor on the Profiles and Parameters at the Target

The Effect of the Magnetic Flux Geometry of a Poloidal Divertor on the Profiles and Parameters at the Target

A. Loarte, P.J. Harbour
and JET Team*

JET-Joint Undertaking, Culham Science Centre, OX14 3DB, Abingdon, UK

** See Appendix 1*

Preprint of Paper to be submitted for publication in
Nuclear Fusion (Letters)

The Effect of the Magnetic Flux Geometry of a Poloidal Divertor on the Profiles and Parameters at the Target.

by

A. Loarte and P.J. Harbour

JET Joint Undertaking, Abingdon, Oxon, OX14 3EA, UK

Abstract. The effect of the magnetic flux geometry of a poloidal divertor on the profiles and parameters at the divertor target is described by means of a simple model. Due to the magnetic flux expansion near the X-point, exponential profiles at the midplane of the tokamak are transformed in Gaussian profiles at the target. When the angle of incidence of the field line onto the target is considered, the possible existence of a maximum in the flux onto the target away from the magnetic separatrix appears naturally in agreement with experimental results.

1. Introduction.

In the scrape-off layer (SOL) of a tokamak the profiles of electron density, $n_e(R)$, and electron temperature, $T_e(R)$, have been shown to decrease with distance, falling smoothly from their values $n_e(a)$, $T_e(a)$ at the magnetic separatrix, and the variation is generally exponential [1, 2, 3]. Although this may be true in the SOL far from a poloidal divertor target, the profiles in the divertor are more complicated, and some parameters, for example the heat and particle fluxes onto the target, may not even show monotonic trends, but they may increase to maxima outside the separatrix and then decrease again; this is especially relevant for open divertors such as those in JET [4, 5] and JT-60 [6] where the divertor target may be very close to the X-point field null. It is the purpose of this paper to show how the magnetic geometry of a tokamak with a poloidal divertor inevitably leads to such profiles and we will show that if the profiles , (eg of density and temperature) in the SOL at the midplane are essentially exponential, then the corresponding profiles at the divertor target are essentially Gaussian. What is more, the profiles of heat and particle fluxes onto the target are essentially skewed Gaussian and have maxima which may be some distance radially outside the separatrix. Our modelling of maxima outside the separatrix depends on the magnetic geometry and not on the existence of exponential profiles in the SOL, indeed any reasonable SOL profile produces a similar result. We ignore effects of magnetic drift and of diffusion into the private flux region of the poloidal divertor; each of these can give rise to maxima which are radially outside the separatrix [5, 7] but our geometrical argument gives rise to such a pronounced effect that the effects of magnetic drift and of diffusion appear as perturbations.

The magnetic argument is based on the behaviour of the magnetic flux, $\psi(R, Z)$, in the SOL, which (for small displacements) varies linearly with the distance from the separatrix everywhere except near the X-point, where it varies

quadratically. For example if we consider a tokamak with an X-point at the top, then at the outer midplane separatrix we may say that if the profiles $n_e(R)$, $T_e(R)$ are exponential functions of R, it follows that they are also exponential functions of ψ. In the divertor the functions $n_e(\psi)$, $T_e(\psi)$ may be taken to be exponential, ignoring gradients parallel to the magnetic field, but in mapping from the midplane to the divertor the spatial profiles of n_e, T_e are transformed into Gaussian profiles.

At the divertor target we are interested in two types of profiles. The first type (A) includes the density and temperature profiles and the related fluxes of particles and energy parallel to the magnetic field; the second type (B) are the profiles of fluxes perpendicular to the target, including energy and particle fluxes onto the target and influxes of recycling and sputtered neutral species. The efflux profiles of type B may be derived from those of type A, which are essentially Gaussian, by multiplying by the sine of the angle between the magnetic field line and the target. This angle increases more or less linearly from zero at or above the X-point and so type B profiles, under the conditions we will describe, are skewed Gaussian with maxima which can be outside the separatrix.

In the next section we describe the magnetic fields, flux surfaces and angles of incidence of the field line onto the target and in the following one we describe the consequences for profiles in the divertor. A more detailed discussion of the effect on plasma and impurity transport is to be published separately and considers the improved retention of intrinsic impurities in the divertor, a consequence of the displacement of the source of sputtered impurities radially outwards in the divertor. In this paper we use an analytical model with cylindrical magnetic geometry to present the argument, noting that it can be readily generalized to toroidal geometry where the magnetic equilibrium is available, the generalization producing no qualitative change in the result [8].

2. Magnetic fields, flux surfaces and angles.

We consider the simplest distribution of currents that presents the characteristics of a poloidal divertor. This is the case of two equal currents (see Fig.1) along two infinite conductors at a vertical distance b from the origin of coordinates, which is at the X-point position, a uniform toroidal field B_T parallel to the currents, and a plane horizontal target located at Z_t. For this simple case the magnetic field is given by

$$B_R(R,Z) = \frac{-\mu_0 I}{\pi} \quad \frac{Z\left(R^2+Z^2-b^2\right)}{\left((Z+b)^2+R^2\right)\left((Z-b)^2+R^2\right)} \tag{1.a}$$

$$B_Z(R,Z) = \frac{\mu_0 I}{\pi} \quad \frac{R\left(R^2+Z^2+b^2\right)}{\left((Z+b)^2+R^2\right)\left((Z-b)^2+R^2\right)} \tag{1.b}$$

$$B_T(R,Z) = B_T, \tag{1.c}$$

and for this field configuration the flux surfaces are obtained as

$$\left(R^2+Z^2\right)^2 + 2\,b^2\,\left(R^2-Z^2\right) = K(\psi), \tag{2}$$

where $K(\psi)$ is a constant for any flux value ψ . These curves are known as the Ovals of Cassini [9]. The magnetic separatrix is defined with $K(\psi) = 0$. The target is intercepted by the separatrix at two magnetic strike points $R_t(K = 0, Z_t) \simeq \pm Z_t$, where $R_t(K(\psi), Z_t)$ is the radial coordinate at the target corresponding to a flux ψ, for the case in which $R_t^2(K(\psi), Z_t) + Z_t^2 << b^2$ (eg in JET, $Z_t < 20\ cm$, $b \simeq 200\ cm$).

Now we can relate a point in the SOL at the midplane to one at the divertor target on the same flux surface. Using Eq. 2 we map radial distances from the separatrix at the midplane ($Z = -b$), to those measured at the target position ($Z = Z_t$) corresponding to the same flux surfaces.

We now use a Taylor expansion for the magnetic flux near the separatrix at the midplane and near the target, for the case in which the distance of a flux surface with flux value ψ from the separatrix (where $K = 0$) , at the midplane, is small compared to b and also $R_t^2(K(\psi), Z_t) + Z_t^2 << b^2$. The expansion is to first order at the midplane and to second order near the target, because the first order vanishes due to the null in the field. We then obtain a simple expression for this mapping

$$R_{mp}(K(\psi), -b) - a = \frac{R_t^2(K(\psi), Z_t) - Z_t^2}{2\,a\,\left(2 + (a/b)^2\right)}, \tag{3}$$

where

$R_{mp}(K(\psi), -b)$ is the radius of the flux surface ψ at the midplane,

$R_t(K(\psi), Z_t)$ is the corresponding radius of the flux surface ψ at the target position, and

a is the radius of the separatrix at the midplane $\left(a = b\ (\sqrt{5} - 2)^{1/2}\right)$.

The linear (midplane) to quadratic (divertor) relationship described in Eq. 3 occurs both in the present simple cylindrical model and in the toroidal equilibria for a tokamak with a poloidal divertor because it depends on the existence of a point of vanishing poloidal field.

For the present simple configuration we obtain an analytical expression for the angle ϕ, between the field line and the target (a flat horizontal target is assumed at $Z = Z_t$) for any point (R_t, Z_t) at the target,

$$\sin \phi(R_t, Z_t) = \frac{-B_Z(R_t, Z_t)}{\sqrt{B_T^2 + B_R^2(R_t, Z_t) + B_Z^2(R_t, Z_t)}}. \tag{4}$$

Eq. 4 can be written more simply for the usual limit valid near the X-point, $B_t^2 >> B_\beta^2$, where B_P is the local poloidal field, and $R_t^2 + Z_t^2 << b^2$

$$\sin \phi(R_t, Z_t) = \frac{-\mu_0 I}{\pi\ |B_T|\ b^2}\ R_t, \tag{5}$$

showing the expected linear increase of this angle when we move radially away from the X-point (for typical values in JET $\sin \phi \simeq \phi$).

3. Consequences for the profiles of the physical parameters in the divertor.

We assume a simple model for the physical parameters in the SOL (although more detailed models could be also used): the temperature is constant along the field line and the density decreases from $n_e(a)$ at the midplane to $n_e(a)/2$ at the target, owing to the acceleration to Mach 1 at the target. The radial dependence of these parameters is assumed to be a decaying exponential profile out from the separatrix, at the midplane, as has been observed in many divertor tokamaks [1, 2, 3]. We then deduce the profiles for the physical parameters at the target as a function of their profiles at the midplane.

3.1 Type A profiles and parameters.

If the profiles for n_e and T_e at the midplane are

$$n_e(R_{mp}) = n_e(a) \exp\left(- \frac{(R_{mp} - a)}{\lambda_n} \right) \tag{6.a}$$

$$T_e(R_{mp}) = T_e(a) \exp\left(- \frac{(R_{mp} - a)}{\lambda_T} \right) \tag{6.b}$$

the corresponding expressions for these profiles at the target are

$$n_e(R_t) = \frac{n_e(a)}{2} \exp\left(\frac{-(R_t^2 - Z_t^2)}{2\,a\,\left(2 + (a/b)^2\right)\lambda_n} \right) \tag{7.a}$$

$$T_e(R_t) = T_e(a) \exp\left(\frac{-(R_t^2 - Z_t^2)}{2\,a\,\left(2 + (a/b)^2\right)\lambda_T} \right) \tag{7.b}$$

where

$R_{mp} = R_{mp}(K(\psi), -b)$,

$R_t = R_t(K(\psi), Z_t)$,

are the radii of the flux surface ψ at the midplane and the target respectively and diffusion into the private flux region is ignored. Hence, the electron and ion flows, **along** the field line, that reach the target, are

$$\Gamma(R_t, Z_t) = \Gamma(a) \exp\left(\frac{-(R_t^2 - Z_t^2)}{2\,a\,\left(2 + (a/b)^2\right)\lambda_\Gamma} \right) \tag{8}$$

where

$$\lambda_\Gamma^{-1} = \lambda_n^{-1} + (2\,\lambda_T)^{-1} \tag{9}$$

would be the equivalent e-folding length for the flows at the midplane (i.e. the e-folding length for the parameter $n_e(R_{mp})\,c_s(R_{mp})$, where c_s is the isothermal sound speed, there being no flows at the point of symmetry). For the energy flow along

the field line we would obtain a similar expression with Γ replaced by P and λ_Γ replaced by λ_P, the equivalent e-folding length for energy flow at the midplane.

From the previous expressions it is clear that in the vicinity of the X-point the physical parameters follow a Gaussian profile as a function of major radius if an exponential one is assumed at the midplane of the tokamak. This is quite different from the exponential law often assumed, which would only be valid if there were a constant flux expansion due to the X-point. It is also important to note that the physical parameters and the flows along the field line present their highest values at the magnetic strike points, $R_t \simeq \pm Z_t$, on the target.

3.2 Type B profiles and parameters.

The energy and particle fluxes onto the target or particle influxes from the target depend on the normal component to the target of the energy/particle flux along the field. For the energy this consideration is straightforward while for the particle flux we must assume that the influxes from the target are, on average , emitted normally. This normal component is determined by

$$\Gamma_\perp(R_t, Z_t) = \Gamma(R_t, Z_t) \mid \sin \phi(R_t, Z_t) \mid . \tag{10}$$

From the expressions derived for the flows along the field line and the angle between the field line and the target it can be shown that the expression for the perpendicular flow presents a local maximum at

$$R_t^{max} = \pm \sqrt{\lambda\, a \left(2 + (a/b)^2\right)}\,, \tag{11}$$

where λ, is the equivalent e-folding length for the considered flow (energy or particle outflux).

Under the assumption of no diffusion into the private flux region, only the points at the target where $|R_t| > Z_t$ receive a finite flow, hence two physical situations are possible:

- With $|R_t^{max}| > Z_t$, the normal flow onto the target presents a local maximum at a position different from that of the magnetic strike points ($R_t \simeq \pm Z_t$), and the position of the local maximum does not depend on the distance from the X-point to the target (Z_t) , provided this is small.

- With $|R_t^{max}| \leq Z_t$, the normal flow onto the target presents its highest value at the magnetic strike points.

This characteristic behaviour of the fluxes along the field line (type A) and onto the target (type B) is shown in Fig. 2. In this figure the effect that the distance between X-point and the target has on these fluxes is shown for typical values for JET ($b = 200cm, I = 3MA, B_T = 2.5T, \lambda_\Gamma = 1cm$). In row a) the magnetic flux surfaces and the target position are shown for various X-point to wall distances. In row b) the normalized profiles for the fluxes along the field line (type A) at the target are shown; these profiles are Gaussian, as is clearly seen when the X-point is very close to the wall, but when the X-point is not close to the wall, as in DIII-D, they could be identified with exponential profiles with an e-folding length given by

$$\lambda_\Gamma^t \simeq \frac{a\left(2+(a/b)^2\right)\lambda_\Gamma}{Z_t}, \qquad (12)$$

for our analytical model. In row c) the sine of the angle between the field line and the target is shown, it displays the expected approximate linear increase with the radial distance from the X-point. In row d) the normalized profiles for the fluxes (type B) onto and effluxes from the target are shown, these profiles are skewed Gaussian. When the X-point is not close to the wall the profiles have their highest values at the magnetic strike points, but when the X-point is close to the wall they have a maximum away from the magnetic strike points and, as also shown, the position of these maxima does not depend on the X-point to wall distance provided this is small enough for the maxima to exist. It is also important to note that the position of these maxima depends, following Eq. 11, on the equivalent e-folding length for the fluxes at the midplane, being closer the smaller the equivalent e-folding length at the midplane, and hence should be affected by the different confinement regimes obtained in the tokamak.

The qualitative behaviour described above is in good agreement with the experimental results from JET shown in Fig. 3. In this figure the radial distance, S^{max}, between the points of maximum influx from the target, deduced from H_α measurements with a CCD camera, is plotted versus the vertical distance from the X-point to the target, Z_t [10], obtained from a local expansion of the magnetic flux and using the poloidal magnetic field measurements in the vicinity of the X-point (XLOC code [11]) ; as this distance is reduced the points of maximum influx move closer until they reach a position that remains approximately unchanged if the X-point to wall distance is reduced further. This minimum separation between the points of maximum influx is smaller when the regime of confinement is H-mode than when it is ohmic as predicted by Eq. 11, noting that the value of the e-folding length for the parameters in the SOL, λ, is smaller with H-mode.

To get a better quantitative agreement with these experimental observations for JET a more realistic, although still simple, magnetic configuration may be used. The D-shaped plasma in JET has two X-point nulls in the poloidal field, not always both inside the vessel. A system of current filaments which simulates this is a configuration of three currents. We consider, for simplicity, three equal and equally spaced current filaments in a plane, the plasma current being the middle one. The calculation is similar to the one already described, although more complicated and the qualitative conclusions are the same. However the quantitative results are in better agreement with the experiment. For this more realistic configuration we find that the position of the local maximum influx occurs at

$$R_t^{max} \simeq \pm\sqrt{\lambda\, a}\,, \qquad (13)$$

about a factor of $\sqrt{2}$ smaller than with the two current model. The better agreement with the experimental results is demonstrated for instance for JET : $a \simeq 100$ *cm*, and the values deduced from Fig.3, $R_t^{max} = 7$ cm (H), 11 cm (OH), give $\lambda_\Gamma = 0.5$ cm (H), 1.2 cm (OH). This is in good agreement with Langmuir probe measurements in the JET SOL [12], despite differences between the geometry in JET and in the simple model.

Although, in experiment, there are also effects such as diffusion into the private flux region and particle drifts from the flux surfaces to be considered, these other effects are estimated to be less important and the relatively good agreement even with the simple models we have shown, suggests that the magnetic geometry effects are dominant.

To summarize, in this paper we have shown that the existence of a null point in the poloidal magnetic field has the effect that the exponential profiles for the physical parameters at the midplane of the tokamak are transformed into Gaussian profiles in the vicinity of the X-point. This fact combined with the low angle of incidence of the field line onto a target located near the null produces a maximum in the power deposition onto the target and in the particle influx from the target that does not coincide with the magnetic strike points on the target if the X-point is close to the wall. The existence of these maxima outside the magnetic strike points is not in contradiction with the assumption that the plasma particles flow along the field lines. While the appearance of a (type B) maximum outside the separatrix is interesting in its own right, the maximum in the influx of both hydrogen and impurities may have important consequences for the flow balance in the vicinity of the divertor target [13].

Acknowledgment : It is a pleasure to acknowledge D.D.R. Summers, L. de Kock, J.A. Tagle, C.G. Lowry, J.D. Callen and D. O'Brien for fruitful discussions. The authors are grateful to D.D.R. Summers for his permission to reproduce unpublished experimental results (Fig. 3).

4. References

[1] TANGA, A., CAMPBELL, D.J., DENNE, B., et al., in Controlled Fusion and Plasma Physics (Proc. 12th Eur. Conf. Budapest, 1985), Vol. 9F, Part I, European Physical Society (1985) 70.

[2] DE KOCK, L., STOTT, P.E., CLEMENT, S., et al., in Plasma Physics and Controlled Nuclear Fusion Research 1988 (Proc. 12th Int. Conf. Nice,1988), Vol.1, IAEA, Vienna (1989) 467.

[3] SHIMOMURA, Y., KEILHACKER, M., LACKNER, K., et al., Nucl. Fusion **23** (1983) 869.

[4] REICHLE, R., SUMMERS, D.D.R., STAMP, M.F., J. Nucl. Mater. **176 & 177** (1990) 375.

[5] O'BRIEN, D.P., KOVANEN, M.A., REICHLE, R., et al., in Controlled Fusion and Plasma Physics (Proc. 17th Eur. Conf. Amsterdam, 1990), Vol. 14B, Part I, European Physical Society (1990) 251.

[6] ITAMI, K., NISHITANI, T., HOSOGANE, N., et al., Proc. Tech. Com. Impurity Control in Toroidal Devices, IAEA-TECDOC-536, (1989) 67.

[7] TSOIS, N., BESSENRODT-WEBERPLAS, M., CARLSON, A., et al., in Controlled Fusion and Plasma Physics (Proc. 16th Eur. Conf. Venice, 1989), Vol. 13B, Part III, European Physical Society (1989) 907; NEUHAUSER, J., (IPP Garching), personal communication, July 1991.

[8] CALLEN, J.D., (University of Wisconsin), personal communication, July 1991.

[9] SPIEGEL, M.R., Mathematical Handbook. McGraw-Hill. New York (1968).

[10] SUMMERS, D.D.R., LESOURD, M., REICHLE, R., et al., in Controlled Fusion and Plasma Physics (Proc. 18th Eur. Conf. Berlin, 1991), Vol. 15C, Part I, European Physical Society (1991) 5.
[11] O'BRIEN, D.P., ELLIS, J., to be published.
[12] TAGLE, J.A., BURES, M., CAMPBELL, D.J., et al., in Controlled Fusion and Plasma Physics (Proc. 18th Eur. Conf. Berlin, 1991), Vol. 15C, Part III, European Physical Society (1991) 93.
[13] HARBOUR, P.J., in Contributions to the 3rd Workshop on H-mode Physics, (JET Joint Undertaking, Abingdon, UK; Ed. M. KEILHACKER, 26 June 1991) Vol. 1, (1991) 185.

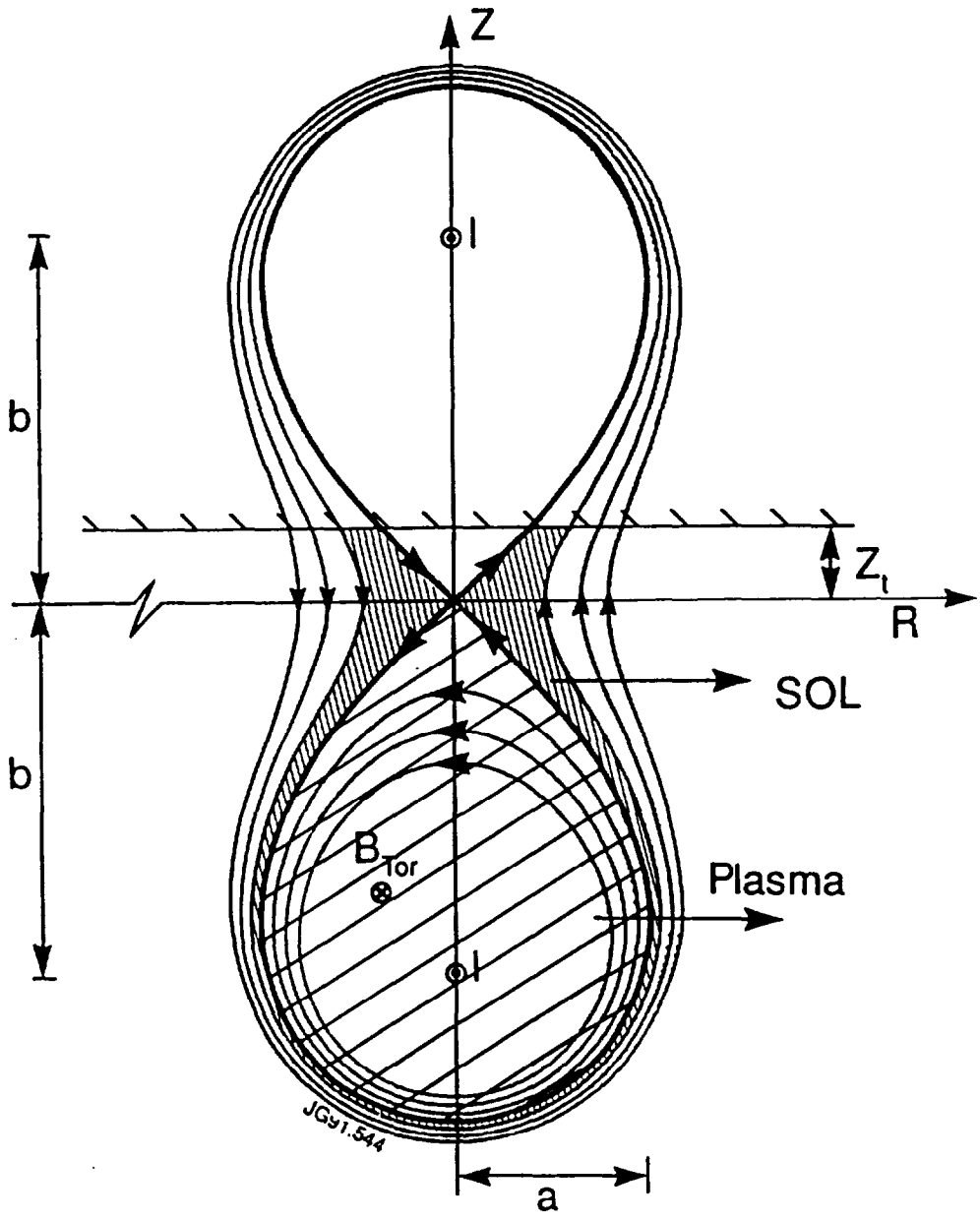

Fig.1. Layout of the magnetic geometry used in the analytical model for the poloidal divertor (Note the strongly nonuniform spacing of the flux surfaces in the vicinity of the X-point).

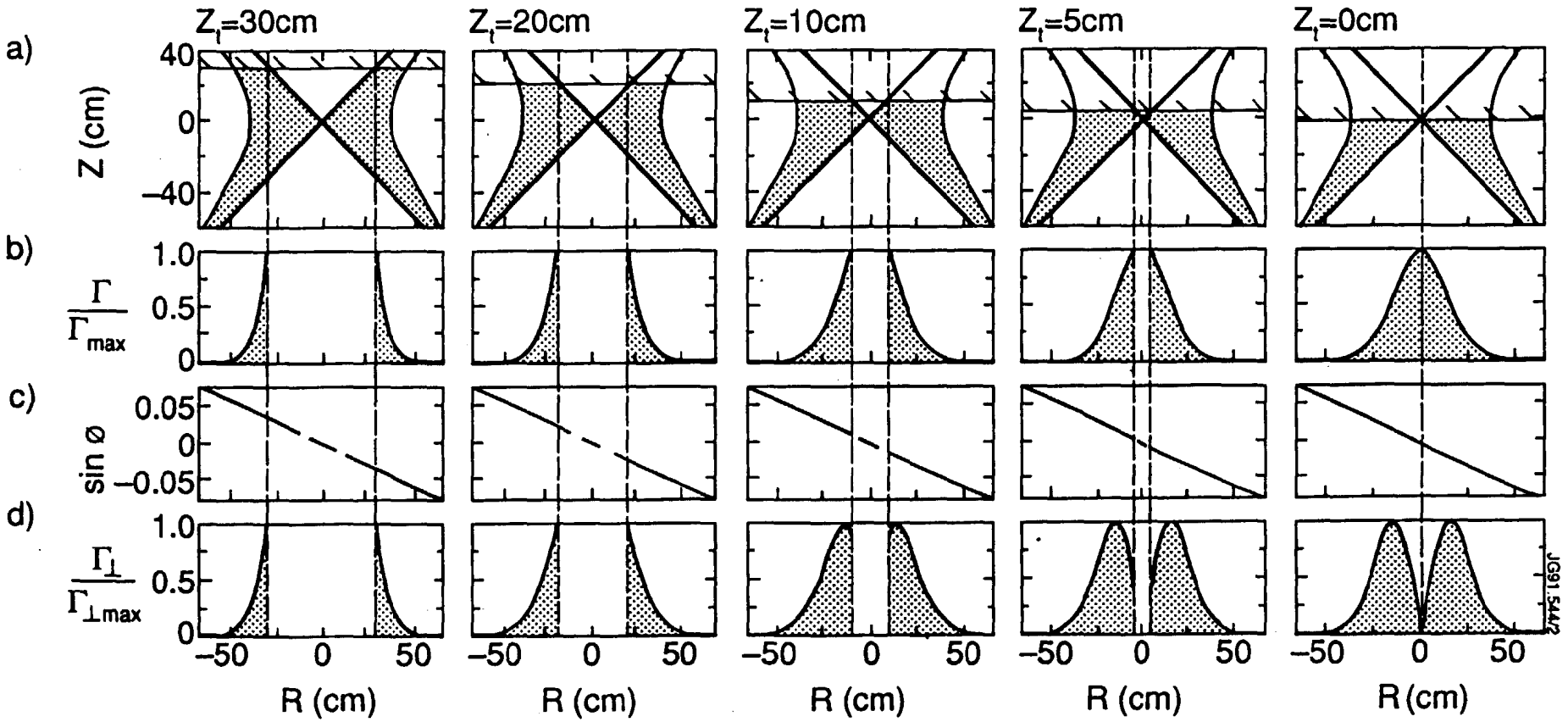

Fig.2. Calculation of the profiles for the parameters for various X-point to wall distances for typical JET values ($b = 200cm$, $I = 3MA$, $B_T = 2.5T$). Row a) shows the magnetic flux surfaces and the target positions for a range of Z_t from 30 cm to zero. Row b) shows the normalized profiles at the target for the fluxes along the field (type A); these profiles are Gaussian with their highest values at the magnetic strike points. Row c) shows sin ϕ (the angle between the field line and the target) at the target, this angle shows an approximately linear increase with the radial distance from the X-point (the dashed part corresponds to the private flux region, which receives no flux in our model). Row d) shows the normalized (type B) profiles for the fluxes onto the target; these profiles are skewed Gaussian and present local maxima (at a position independent of the X-point to wall distance) away from the magnetic strike points ($R_t \simeq \pm Z_t$), if the X-point is close to the wall. The horizontal axis in Row a) is the Radial axis, in the other Rows this Radial coordinate corresponds to the target (R_t).

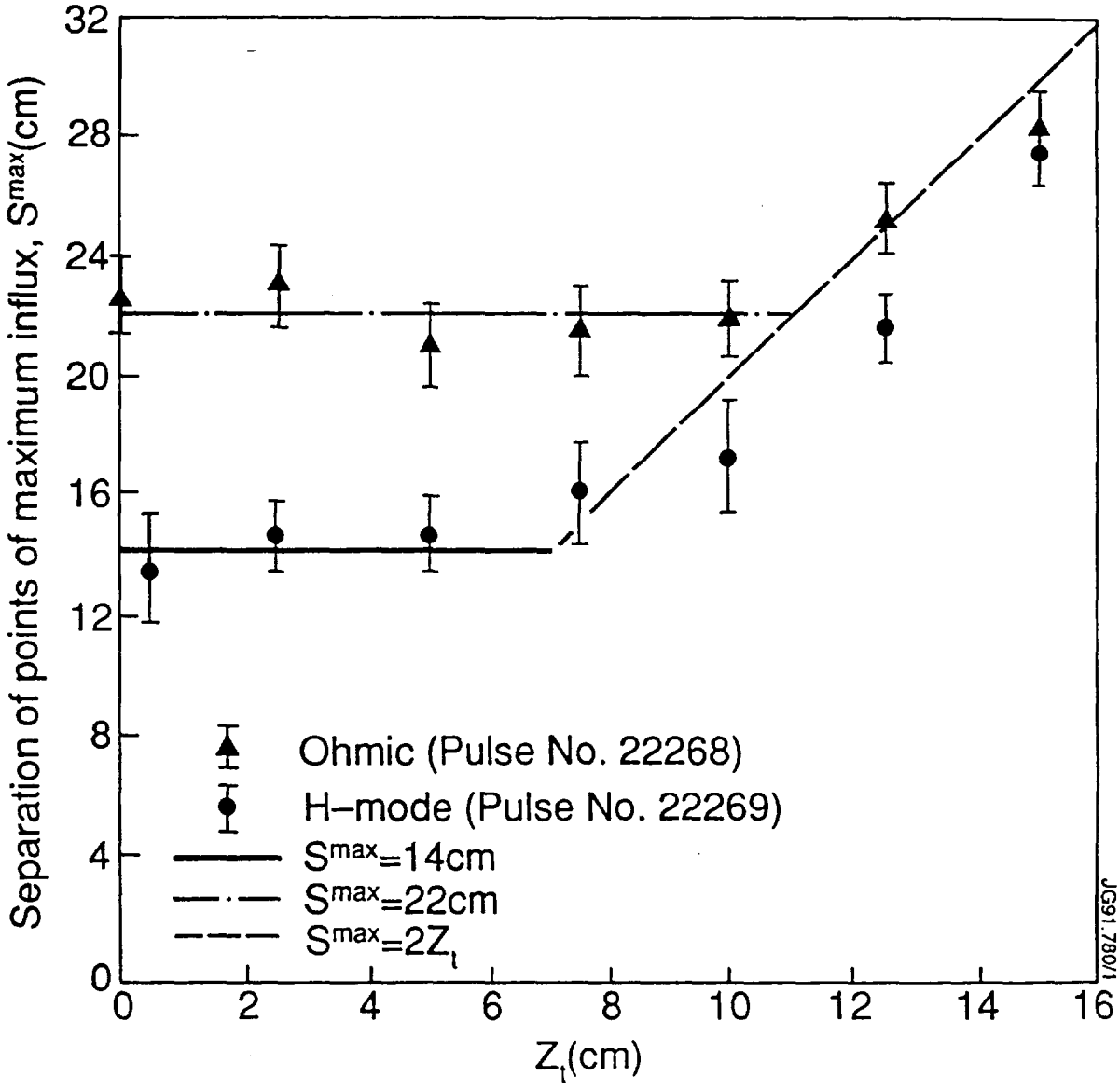

Fig.3. Distance, S^{max}, separating the points of maximum influx from the target in JET (obtained from measurements with a CCD camera and filter of the intensity of H_α radiation [10]) versus X-point to wall distance, Z_t. This distance decreases when the X-point is moved closer to the wall until a separation is reached at which it subsequently remains fairly constant. The minimum separation is smaller in H-mode. The horizontal lines are theoretical predictions from the simple model for the condition $S^{max} = 2\, R_t^{max}$ and using Eq.(13) with $\lambda_\Gamma =$ 0.5 cm (H), 1.2 cm (OH). The diagonal line corresponds to the predicted distance between magnetic strike points, $S^{max} = 2\, Z_t$.

Appendix I

THE JET TEAM

JET Joint Undertaking, Abingdon, Oxon, OX14 3EA, U.K.

J.M. Adams[1], H. Altmann, A. Andersen[14], P. Andrew[18], M. Angelone[29], S.A. Arshad, W. Bailey, P. Ballantyne, B. Balet, P. Barabaschi, R. Barnsley[2], M. Baronian, D.V. Bartlett, A.C. Bell, I. Benfatto[5], G. Benali, H. Bergsaker[11], P. Bertoldi, E. Bertolini, V. Bhatnagar, A.J. Bickley, H. Bindslev[14], T. Bonicelli, S.J. Booth, G. Bosia, M. Botman, D. Boucher, P. Boucquey, P. Breger, H. Brelen, H. Brinkschulte, T. Brown, M. Brusati, T. Budd, M. Bures, T. Businaro, P. Butcher, H. Buttgereit, C. Caldwell-Nichols, D.J. Campbell, P. Card, G. Celentano, C.D. Challis, A.V.Chankin[23], D. Chiron, J. Christiansen, C. Christodoulopoulos, P. Chuilon, R. Claesen, S. Clement, E. Clipsham, J.P. Coad, M. Comiskey[4], S. Conroy, M. Cooke, S. Cooper, J.G. Cordey, W. Core, G. Corrigan, S. Corti, A.E. Costley, G. Cottrell, M. Cox[7], P. Cripwell, H. de Blank[15], H. de Esch, L. de Kock, E. Deksnis, G.B. Denne-Hinnov, G. Deschamps, K.J. Dietz, S.L. Dmitrenko, J. Dobbing, N. Dolgetta, S.E. Dorling, P.G. Doyle, D.F. Düchs, H. Duquenoy, A. Edwards, J. Ehrenberg, A. Ekedahl, T. Elevant[11], S.K. Erents[7], L.G. Eriksson, H. Fajemirokun[12], H. Falter, D. Flory, J. Freiling[15], C. Froger, P. Froissard, K. Fullard, M. Gadeberg, A. Galetsas, D. Gambier, M. Garribba, P. Gaze, R. Giannella, A. Gibson, R.D. Gill, A. Girard, A. Gondhalekar, C. Gormezano, N.A. Gottardi, C. Gowers, B.J. Green, R. Haange, G Haas, A. Haigh, G. Hammett[6], C.J. Hancock, P.J. Harbour, N.C. Hawkes[7], P. Haynes[7], J.L. Hemmerich, T. Hender[7], F.B. Herzog, R.F. Herzog, J. Hoekzema, J. How, M. Huart, L Hughes, T.P. Hughes[4], M. Hugon, M. Huguet, A. Hwang[7], B. Ingram, M. Irving, J. Jacquinot, H. Jaeckel, J.F. Jaeger, G. Janeschitz[13], S. Jankowicz[22], O.N. Jarvis, F. Jensen, E.M. Jones, L.P.D.F. Jones, T.T.C. Jones, J-F. Junger, E. Junique, A. Kaye, B.E. Keen, M. Keilhacker, G.J. Kelly, W. Kerner, R. Konig, A. Konstantellos, M. Kovanen[20], G. Kramer[15], P. Kupschus, R. Lässer, J.R. Last, B. Laundy, L. Lauro-Taroni, K. Lawson[7], M. Lennholm, A. Loarte, R. Lobel, P. Lomas, M. Loughlin, C. Lowry, B. Macklin, G. Maddison[7], G. Magyar, W. Mandl[13], V. Marchese, F. Marcus, J. Mart, E. Martin, R. Martin-Solis[8], P. Massmann, G. McCracken[7], P. Meriguet, P. Miele, S.F. Mills, P. Millward, R. Mohanti[17], P.L. Mondino, A. Montvai[3], S. Moriyama[28], P. Morgan, H. Morsi, G. Murphy, M. Mynarends, R. Myrnäs[16], C. Nardone, F. Nave[21], G. Newbert, M. Newman, P. Nielsen, P. Noll, W. Obert, D. O'Brien, J. O'Rourke, R. Ostrom, M. Ottaviani, M. Pain, F. Paoletti, S. Papastergiou, D. Pasini, A. Peacock, N. Peacock[7], D. Pearson[12], R. Pepe de Silva, G. Perinic, C. Perry, M. Pick, R. Pitts[7], J. Plancoulaine, J-P. Poffé, F. Porcelli, L. Porte[19], R. Prentice, S. Puppin, S. Putvinsko[23], G. Radford[9], T. Raimondi, M.C. Ramos de Andrade, P-H. Rebut, R. Reichle, E. Righi, F. Rimini, D. Robinson[7], A. Rolfe, R.T. Ross, L. Rossi, R. Russ, P. Rutter, H.C. Sack, G. Sadler, G. Saibene, J.L. Salanave, G. Sanazzaro, A. Santagiustina, R. Sartori, C. Sborchia, P. Schild, M. Schmid, G. Schmidt[6], B. Schunke, S.M. Scott, A. Sibley, R. Simonini, A.C.C. Sips, P. Smeulders, R. Stankiewicz[27], M. Stamp, P. Stangeby[18], D.F. Start, C.A. Steed, D. Stork, P.E. Stott, T.E. Stringer, P. Stubberfield, D. Summers, H. Summers[19], L. Svensson, J.A. Tagle[21], A. Tanga, A. Taroni, A. Tesini, P.R. Thomas, E. Thompson, K. Thomsen, J.M. Todd, P. Trevalion, B. Tubbing, F. Tibone, E. Usselmann, H. van der Beken, G. Vlases, M. von Hellermann, T. Wade, C. Walker, R. Walton[6], D. Ward, M.L. Watkins, M.J. Watson, S. Weber[10], J. Wesson, T.J. Wijnands, J. Wilks, D. Wilson, T. Winkel, R. Wolf, B. Wolle[24], D. Wong, C. Woodward, Y. Wu[25], M. Wykes, I.D. Young, L. Zannelli, Y. Zhu[26], W. Zwingmann.

PERMANENT ADDRESSES

1. UKAEA, Harwell, Didcot, Oxon, UK.
2. University of Leicester, Leicester, UK.
3. Central Research Institute for Physics, Academy of Sciences, Budapest, Hungary.
4. University of Essex, Colchester, UK.
5. ENEA-CNR, Padova, Italy.
6. Princeton Plasma Physics Laboratory, New Jersey, USA.
7. UKAEA Culham Laboratory, Abingdon, Oxon, UK.
8. Universidad Complutense de Madrid, Spain.
9. Institute of Mathematics, University of Oxford, UK.
10. Freien Universität, Berlin, F.R.G.
11. Swedish Energy Research Commission, S-10072 Stockholm, Sweden.
12. Imperial College of Science and Technology, University of London, UK.
13. Max Planck Institut für Plasmaphysik, Garching bei München, FRG.
14. Risø National Laboratory, Denmark.
15. FOM Instituut voor Plasmafysica, 3430 Be Nieuwegein, The Netherlands.
16. University of Lund, Sweden.
17. North Carolina State University, Raleigh, NC, USA
18. Institute for Aerospace Studies, University of Toronto, Downsview, Ontario, Canada.
19. University of Strathclyde, 107 Rottenrow, Glasgow, UK.
20. Nuclear Engineering Laboratory, Lapeenranta University, Finland.
21. CIEMAT, Madrid, Spain.
22. Institute for Nuclear Studies, Otwock-Swierk, Poland.
23. Kurchatov Institute of Atomic Energy, Moscow, USSR
24. University of Heidelberg, Heidelberg, FRG.
25. Institute for Mechanics, Academia Sinica, Beijing, P.R. China.
26. Southwestern University of Physics, Leshan, P.R. China.
27. RCC Cyfronet, Otwock Swierk, Poland.
28. JAERI, Naka Fusion Research Establishment, Ibaraki, Japan.
29. ENEA, Frascati, Italy.

At 1st June 1991